International Journal of Technology 13(3) 473-483 (2022)
Received May 2019 / Revised May 2020 / Accepted January 2020

International Journal of Technology

http://ijtech.eng.ui.ac.id

Investigation on Weld Characteristic, Welding Position, Microstructure, and Mechanical Properties in Orbital Pulse Current Gas Tungsten Arc Welding of AISI 304L Stainless Steel Pipe

Agus Widyianto[1], Ario Sunar Baskoro[2*], Gandjar Kiswanto[2]

[1]*Department of Automotive Engineering Education, Faculty of Engineering, Universitas Negeri Yogyakarta, Jl. Colombo No.1, Karang Gayam, Caturtunggal, Kab. Sleman 55281, Indonesia*
[2]*Department of Mechanical Engineering, Faculty of Engineering, Universitas Indonesia, Jl. Prof. Dr. Sumitro Djojohadikusumo Kampus UI Depok 16424, Indonesia*

Abstract. Orbital pipe welding is carried out in this study by Pulse Current Gas Tungsten Arc Welding (PC-GTAW) without metal filler (autogenous) of AISI 304L stainless steel pipe. The dimensions of the specimen are 114 mm outside diameter and the thickness of 3 mm. This study investigates the effect of pulse current parameters, weld position, and pulse width on the characteristics of weld geometry, mechanical properties, and microstructure. The welding method used in this study is the continuous current and pulse current. The mean current of each parameter is the same at 100 ± 0.5 Amperes, but in the pulse current, there are variations in peak current, base current, peak current time, and the base current time. The welding speed used is constant at 1.4 mm/s. The result of weld geometry on the outside of pipe has shown that the flat (0°) position is concave and the overhead (180°) position is convex due to the influence of gravity. The microstructure indicates that the fine cellular dendritic structures appear at PC-GTAW. The PC-GTAW can produce good mechanical properties such as the tensile strength and the micro-hardness. The tensile strength of the specimen is reduced 14.23 % from the base metal at parameter 65-B and the flat position.

Keywords: Orbital pipe welding; PC-GTAW; AISI 304L; Weld characteristic

1. Introduction

Austenitic stainless steel (ASS) is a type of material that is widely used in manufacturing. This material is used in the manufacture of pipes, power plants, refineries, pressure vessels, nuclear reactors, automobiles and offshore structures (Karunakaran, 2012). AISI 304L and 316L stainless steel is the type of ASS materials often used in the industry (Alcock & Baufeld, 2017; Jujur et al., 2015). One of the advantages of this material is that it has corrosion-resistant properties at high temperatures and high pressures and has good mechanical properties (Xu et al., 2017). In general, welding of austenitic stainless steel can be performed by using Gas Tungsten Arc Welding (GTAW) or Gas Metal Arc Welding (GMAW). Gas Tungsten Arc Welding (GTAW) is one of the most widely used welding methods used in industrial sectors due to its ability to join materials such as similar or dissimilar metal materials connected with high-quality joints. During the welding process, the specimen melts due to the heat from the welding arc generated process, the

*Corresponding author's email: ario@eng.ui.ac.id, Tel.: +62-21-7270032; Fax: +62-21-7270033
doi: 10.14716/ijtech.v13i3.3134

specimen melts due to the heat from the welding arc generated between the non-consumable tungsten electrodes (Kou, 2003).

Welding of 304L stainless steel alloy using GTAW without added (autogenous) material is susceptible to the phenomenon of hot cracking. Hot cracks are cracks due to heat during the welding process and the type of welded joint (James et al., 2020). Many researchers have studied on hot cracking that often occurs in austenitic stainless steels (Alcantar-Modragón et al., 2021; James et al., 2020; Mirshekari et al., 2014). One method to reduce hot cracking in GTAW welding is to use pulse current.

The depth of penetration and width of the weld bead are factors that can directly affect weld quality. In the GTAW process, it can be increased by raising the weld current. However, an increase in weld current can result in an increase in distortion due to the high heat input (Okano & Mochizuki, 2017). Stainless steel, especially the austenite stainless steel (ASS) type, has the highest thermal expansion coefficient and the lowest thermal conductivity compared to carbon steel and other alloy steel (Tseng & Hsu, 2011). One other method to reduce the heat input that occurs due to an increase in weld current is by welding pulse current (Pal & Pal, 2011). With pulse current welding, many parameters can be set including peak current, base current, time peak current, and time base current (Dorn et al., 2009). In orbital pipe welding, the use of pulse currents can reduce the effect of gravity during the welding process.

In previous research, Aesh (Aesh, 2007) reported on welding with the continuous current to observe the weld geometry on GTA welding, Gunaraj and Murugan (2000) on SMA welding. Pipe welding has been carried out by researchers such as Lothongkum et al. (2001) studied on orbital welding of stainless steel and the influence of pulsed current on microstructure and weld bead quality. The variation in the welding process and welding parameter to improve the weld characteristics of 304LN stainless steel pipe have been reported by Kulkarni et al. (2008). Baskoro et al. (2011) developed a system to detect and control the weld penetration from the weld pool and optimize it with PSO and GA. Karunakaran (2012) stated that the results of mechanical properties from welding with pulsed current were higher than the continuous current. In addition, the use of pulsed current can reduce porosity and reduce residual stress that occurs after the welding process (Kulkarni et al., 2008). The results of a review conducted by Pal Kamal & Pal Surjya K. (2011) stated that welding with the pulsed current is one method to reduce the heat input received by the material. The choice of pulsed current parameters is crucial due to this will determine the characteristics of the weld bead formed during the welding process (Palani & Murugan, 2006). The effect of pulsed current at the welding position of 6-12 h has been reported by Lothongkum et al. (2001). Next, Daniel et al. (Figueirôa et al., 2017) indicated that the welding position affects the weld geometry and mechanical properties of low carbon steel. The welding position can determine the welding results visually on the orbital pipe welding if the pipe was seen from a horizontal orientation.

Several of the above studies show that the use of welding methods with pulsed currents has a positive impact on weld geometry and mechanical properties. Most of the above studies only vary the pulse current regardless of the magnitude of the heat input or the average current. This affects the weld geometry that was formed and its mechanical properties. Therefore, based on the above research, no research pays attention to the amount of heat input and the mean current in the use of pulse currents in orbital pipe welding. In orbital pipe welding, there is a welding position that needs attention due to the influence of gravity. So, the use of pulsed currents is suitable for reducing the effect of gravity, and the weld geometry can still be controlled. Stainless steel pipe type 304L (AISI 304L) is used in this study. This material is widely used in industries due to it has corrosion-resistant properties. Therefore, further investigation is needed on the effect of orbital pipe welding on weld characteristics, mechanical properties, and microstructure of each welding position.

2. Methods

The material used in this study was AISI 304L stainless steel pipe with an outer diameter of 114.2 mm and a thickness of 3 mm. The optical emission spectrometer (OEM) was used to test the chemical composition of AISI 304L stainless steel pipe, and the chemical composition was listed in Table 1.

Table 1 Chemical composition (wt %) of AISI 304L pipe

	C	Si	Mn	P	S	Cr	Mo
AISI 304L	0.026	0.400	1.44	0.037	0.011	19.5	0.118
	Ni	Al	Cu	Nb	Ti	V	Fe
	8.26	0.006	0.096	0.018	0.002	0.078	bal.

Before welding, the surfaces of all specimens were cleaned by 80 until 400 grit flexible sandpapers. After that, it was cleaned with acetone solution to remove surface impurities (Widyianto et al., 2020). The dimension of a specimen before welding was 1000 mm in length, 114.2 mm in outer diameter, and 3 mm in thickness (Figure 1). After one welding process is complete, the specimen will be left idle until the temperature reaches room temperature. Then, after the entire the welding process was completed, the specimen was cut 125 mm in length, and there were eight parts of the pipe.

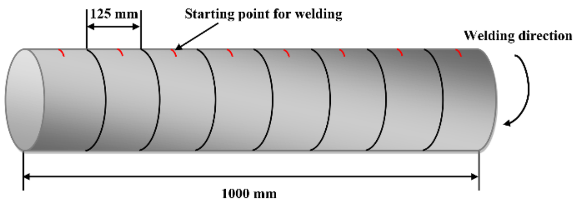

Figure 1 Schematic of specimen preparation

The welding method used in this study was without filler metal (autogenous), without joint two pipes, and using orbital pipe welding. A GeKaMac power TIG 2200 DC pulse welding machine was used in this study with 1 phase input voltage, 230 V, 50-60 Hz, and current range 5-220 A. The top weld zone was shielded by high purity argon (99.99%) gas with a flow rate of 11 L/min. A tungsten electrode was used EWTh-2 with a red code AWS with a diameter 2.4mm and a sharpening angle of 30°. The welding speed was set constant 1.40mm/s. The weld parameters used in this study are shown in Table 2.

Table 2 Welding parameters GTAW process

Parameter	Value
Resource	DCEN
Welding current	40 - 212 Ampere
Welding speed	1.4 mm/s
Electrode type	EWTh-2
Electrode diameter	2.4 mm
Nominal arc length	3 mm
Shielding gas	99.99% Argon
Shielding gas flow rate	11 L/min

A pulsed and continuous current method was adopted in the GTAW process, with variations of peak currents, base currents, and pulse widths. At pulsed and continuous currents, the GTAW average current was 100 ± 0.5 amps and the average excitation voltage during welding was 11-13 volts. In addition, the heat input calculation was performed through the material during pulsed current welding. Heat input in the pulsed current GTAW can be calculated from the mean current; meanwhile, heat input in the continuous current GTAW can be calculated from the continuous current, where, V, Im, S, and η are voltage, mean current, welding speed, and arc efficiency (usually assumed to be 60 % for pulse GTAW) (Giridharan & Murugan, 2009), respectively.

The value of mean current (I_m) can be calculated by using Equation 1 (Giridharan & Murugan, 2009):

$$I_m = \frac{I_p\, t_p + I_b\, t_b}{t_p + t_b} \quad (1)$$

where, I_p, I_b, t_p, and t_b are peak current, base/background current, time peak current and time base current, respectively. Figure 2 shows the schematic illustration of the pulsed current.

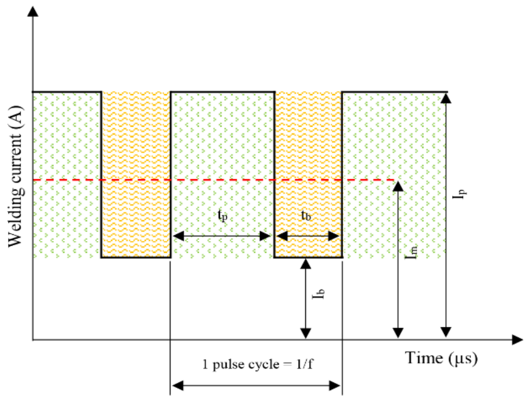

Figure 2 Schematic illustration of pulsed current (Widyianto et al., 2020)

The pulsed and continuous currents GTAW process parameters that will be studied was presented in Table 3. Codes A, B and C have the meaning of low, medium and high peak currents with variations in pulse width, respectively.

Table 3 Pulsed and continuous current GTAW process parameters

No	Code	Peak current (A)	Base current (A)	Peak time (ms)	Base time (ms)	Pulse width (%)	Mean current (A)	Mean voltage (V)	Heat input (kJ/mm)
1	35-A	138	80	70	130	35	100.3	12.20	524.43
2	35-B	175	60	70	130	35	100.25	12.05	517.72
3	35-C	212	40	70	130	35	100.2	11.75	504.58
4	50-A	120	80	100	100	50	100	12.25	525.00
5	50-B	140	60	100	100	50	100	12.25	525.00
6	50-C	160	40	100	100	50	100	12.00	514.29
7	65-A	111	80	130	70	65	100.15	12.15	521.50
8	65-B	122	60	130	70	65	100.3	12.30	528.72
9	65-C	133	40	130	70	65	100.45	12.28	528.44
10	100-A	-	-	-	-	-	100	13	557.14

Weld characteristics can be determined with the width bead. Measurement of the top bead width was performed to determine the characteristics of the weld bead formed during the welding process. The top bead width was measured, starting from 0° to 300° with increment 15°, and there were 21 measurement points. The measurement was examined with a Dino-Lite digital microscope. The specimen was cut in cross section and the weld shape at each weld position was investigated. The specimen preparation was required for this process, including sanding with wet sandpapers with a distribution of 240, 600, 800, and 1500 grit. After that, the specimen was polished with a combination of titanium (IV) oxide and ethanol. The specimen was etched using a combination of 5 ml HNO3, 5 ml HCl, 1 gr picric acid, and 200 ml ethanol. Macrostructure observations were performed using a Dino-Lite digital microscope to investigate the weld geometry.

The tensile tests were performed using Tensilon RTF-2350 Universal Testing Machine with a maximum load of 50kN at a constant crosshead velocity of 5 mm/min. The specimens were prepared with a standard of ASTM E-8M (Figure 3a) (Kusuma et al, 2017). Micro-hardness measurement was performed by using a Mitutoyo 810 Vickers Micro Hardness Testing Machine with standard ASTM E384 (Purnama et al., 2020). The measurement of micro-hardness with a load of 500 gr for a dwell time of 15 s in four zones of weld joint of base metal (BM), heat affected zone (HAZ), partially melted zone (PMZ) and weld metal (WM). There were three indentations at 250 µm intervals in the four zones of weld joint of BM, HAZ, PMZ and WM (Figure 3b). The indentations were made on the horizontal distribution.

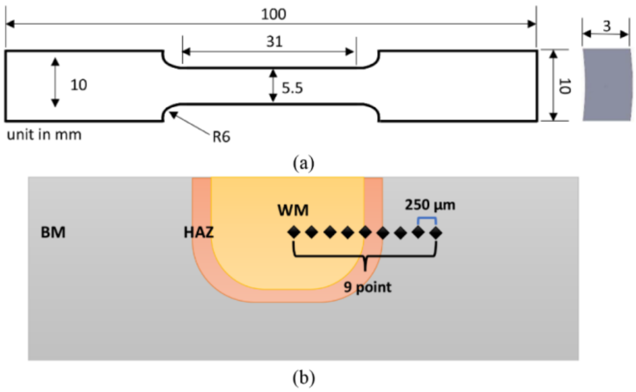

Figure 3 Schematic illustration of (a) tensile test and (b) microhardness test specimen

Microstructure observations were carried out using an Olympus GX51 optical microscope. The specimen preparation was performed according to standard metallography procedures and etched using a combination of 5 mL HNO_3, 5 mL HCl, 1 g picric acid, and 200 mL ethanol, to bring up the microstructure features. The BM, HAZ, PMZ, and WM welded joint zones are analyzed for the microstructure formed.

3. Results and Discussion

3.1. Weld Characteristic and Macrostructure

The weld characteristics can be investigated from the width bead. The weld surface profile of the orbital pipe welding shown is in Figure 4a. Figure 4b shows the influence of pulsed currents (peak currents) and pulse widths to the top bead width. Increasing the peak current (I_p) in pulsed current can raise the average width of the top bead, while raising the pulse width can decrease the average width of the top bead. In 65-A parameter can produce above average grain widths that are smaller than other parameters. Peak current (I_p) was the current level used to spray transfer droplets and melt the base material (Palani & Murugan, 2006). The higher peak current will make the weld bead profile wider and deeper.

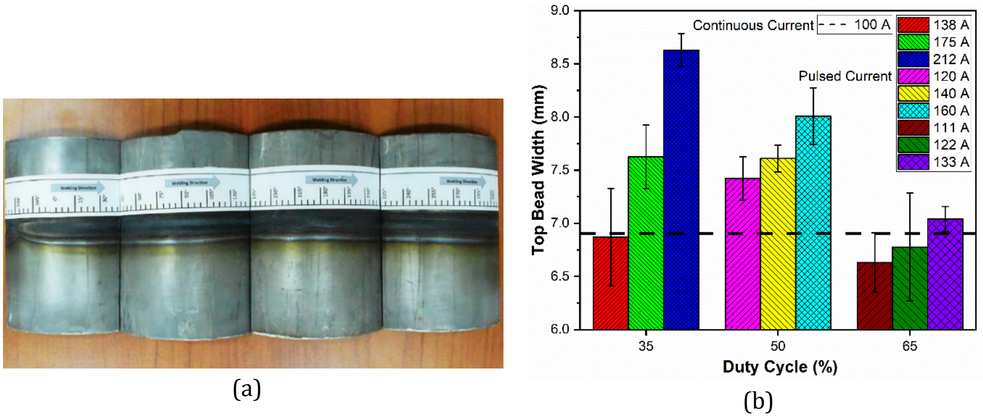

Figure 4 (a) Photograph of the welding surface and (b) Top bead width on various pulse width and pulsed current

The weld geometry in each welding position would be different. Figure 5 shows the weld geometry in different welding positions and parameters. When the welding was in the welding position 0°, the melt material tended to fall so that the weld geometry on the outside of the pipe was concave, and at the welding position of 180° melt material tended to fall as well, and the weld geometry on the outside of the pipe was flat or convex. And at the welding positions of 90° and 270° produces a weld geometry that tends to be flat on the outside of the pipe. The weld geometry at the welding positions of 0° and 180° was strongly influenced by gravity, while the welding positions of 90° and 270° weren't affected by gravity (Figueirôa et al., 2017). In addition, the welding current that was used also affects the impulse that occurs in the material during the welding process, which causes different penetration (Kumar et al., 2016).

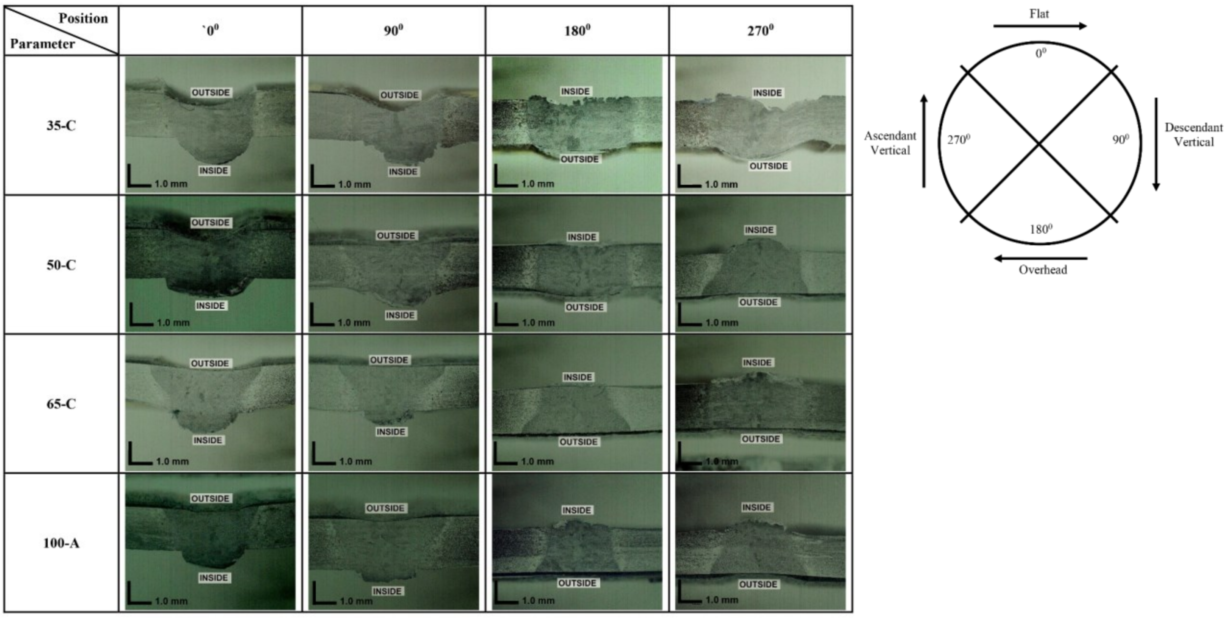

Figure 5 Weld geometry in different parameters and positions

3.2. *Microstructure Analysis*

Microstructure analysis in a different zone of pulsed current (PC) and continuous current (CC) weld joint was presented in Figure 6. The specimen parameters were the parameters 50-C and 100-A in the welding position 0°. Figures 6a and b show the differences in microstructural regions formed, such as heat-affected zone (HAZ), partially melted zone (PMZ), and weld metal zone (WM) with PC-GTAW and CC-GTAW weld joint.

The width of the HAZ region produced by PC was smaller than that of CC. The microstructure in the HAZ region was different from the BM region.

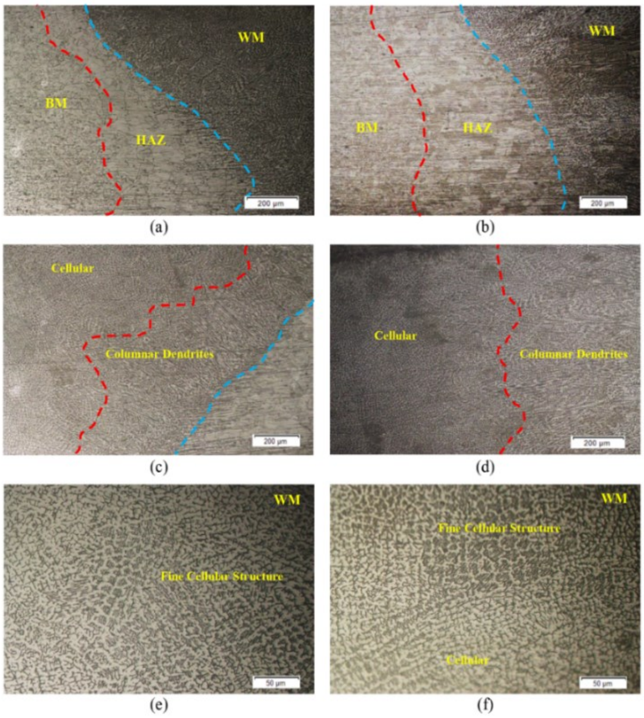

Figure 6 Microstructure in different zones of weld joints produced by PC-GTAW and CC-GTAW (a, b) interface BM, HAZ, and WM, (c, d) weld metal region/near PMZ, and (e, f) center of weld metal region

In the HAZ region, chromium carbide content appears due to during the welding process, rapid cooling occurs. High chromium carbide content on AISI 304L will affect corrosion resistance and fatigue resistance (Casalino et al., 2018). The PMZ region was the region close to the fusion line. Equiaxed grains size in the PMZ area was smaller than in the HAZ region. In addition, in the PMZ area, there was also a decrease in micro-hardness value. Figures 6c and d show the microstructure in the weld metal/near HAZ. The PC-GTAW and CC-GTAW can be an observed amount of columnar dendritic structures and amount cellular dendritic structures. The columnar dendritic structure produced by PC-GTAW was smaller than that of CC-GTAW. The fine cellular dendritic structures can be observed in the center of welds in PC-GTAW and CC-GTAW (Figures 6e and f). The PC-GTAW can produce more fine cellular dendritic structures than CC-GTAW. This was due to the PC-GTAW produce better cooling, which affects the decrease in temperature (Manikandan et al., 2014).

3.3. Tensile Properties

The ultimate tensile strength (UTS) was plotted in different welding parameters and welding positions (Figure 7). Figure 7a, b, c, and d represent the UTS in welding positions of 0°, 90°, 180°, and 270°, respectively. The UTS of each welding position wasn't much different from the BM. The 65-A parameter with the welding position of 180° has the highest UTS among other parameters and welding positions, 703.20 MPa. While, in parameter 65-B with weld position of 0°, has the lowest UTS among other parameters and weld positions, at 508.14 MPa. It shows the strength was reduced by 14.23% from BM. Most of the fracture locations occur in the WM, in the middle, or rather the edge of the WM. Some parameters show a lower tensile strength due to the influence of the weld geometry that was formed too concave, so the area is getting smaller, and there is a decrease in strength.

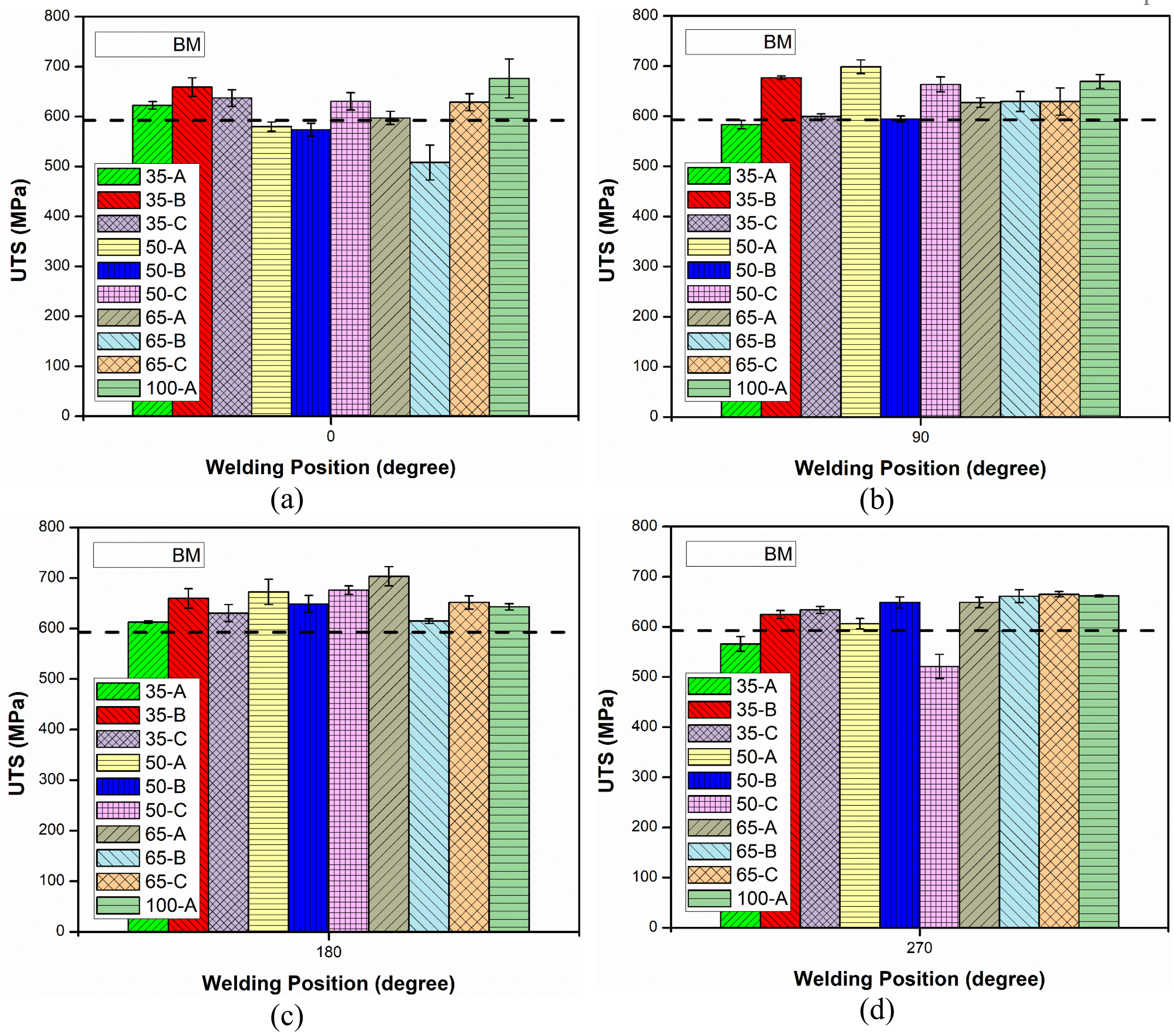

Figure 7 Ultimate tensile strength (UTS) in different parameters and welding positions: (a) 0°, (b) 90°, (c) 180°, and (d) 270° in comparison to base metal (BM)

The material receives the heat input affects the tensile strength. The welding with pulsed current can produce better tensile strength than continuous current (Karunakaran, 2012; Kulkarni et al., 2008). Kumar et al. (2007) reported that the heat input produced from pulsed current can affect tensile properties. In the pulsed current, the heat input can control by adjusting the peak current, the base current, and the pulse width.

3.4. Micro-hardness

Vickers indentations performed Micro-hardness on the specimen of metallographic. The specimens tested for micro-hardness were in parameters 50-C (pulsed current) and 100-A (continuous current) with four welding positions. Figure 8a shows the horizontal distribution of micro-hardness at the 50-C in the BM, HAZ, PMZ and WM sections. Each of the welding positions has different hardness values. The maximum hardness value of weld metal (WM) was 457.8 HV in the welding position of 180°, and the minimum hardness value was 346.2 HV in welding positions of 0° and 270°. In partially melted zone (PMZ) it has the lowest hardness value due to it is near the fusion line. The lowest hardness value was 308.2 HV in the welding position of 270° in PMZ. Afterward, the hardness value increased in the heat-affected zone (HAZ). The maximum hardness value was 494.5 HV in the welding position of 180°. And in the base metal (BM) has a hardness value of 475.6 HV in the welding position of 180°.

Figure 8b shows the horizontal distribution of micro-hardness in parameter 100-A in the BM, HAZ, PMZ, and WM sections. The maximum hardness value of WM was 450.8 HV in the welding position of 270°, and the minimum hardness value was 300.4 HV in welding positions of 90°. The hardness value has decreased in PMZ, and the hardness value in this zone was 261.4 HV in the welding position of 270°. Entering HAZ, the hardness value has increased again. The maximum hardness value in HAZ was 474.6 HV in welding positions of 180° and 270°.

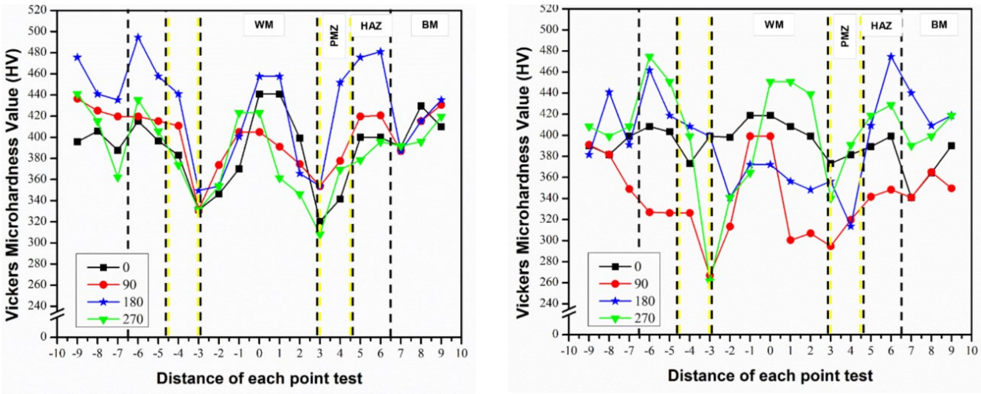

(a) (b)

Figure 8 Micro-hardness value of horizontal distribution across BM, HAZ, PMZ and WM at four welding positions in parameter (a) 50-C and (b) 100-A

Karunakaran (2012) reported that pulsed current has an influence on micro-hardness value. This was due to the peak temperature reached in the pulsed current and continuous current differently. The continuous current has a peak temperature higher than the pulsed current, which can cause the micro-hardness value to decrease (Karunakaran, 2012). In addition, the welding positions also affect micro-hardness value. The pulsed current decreases at the weld positions of 90° to 270°, and increases at the weld positions 270° to 90° (Lothongkum et al., 2001). This will be affected by the peak temperature to be achieved at each welding position.

4. Conclusions

This study investigates the effect of orbital PC-GTAW on weld characteristics, welding position, microstructure, and mechanical properties of AISI 304L stainless steel pipe. In the orbital pipe welding, the weld geometry on the flat (0°) and overhead (180°) positions were strongly influenced by gravity. However, in the descendant vertical (90°) and ascendant vertical (270°) positions weren't too affected by gravity. The weld geometry on the outside of the pipe formed at the flat (0°) position was concave, at the overhead (180°) position was convex, and at the descendant vertical (90°) and ascendant vertical (270°) positions it tends to be flat. The higher the peak current, the geometry of the weld formed will be deeper in penetration at several pipe positions in the orbital pipe welding. PC-GTAW can produce smaller width of HAZ than CC-GTAW due to in the PC-GTAW, the cooling rate is faster, and heat input can be controlled. The orbital PC-GTAW of AISI 304L produced good mechanical properties. The tensile strength of each parameter and welding position was not much different from the base metal, the largest decrease in the parameter 65-B at the flat (0°) position of 14.23% from BM. The micro-hardness value will rise when in the HAZ region, and then it will descend when entering the PMZ region and back up again when in the WM region. The micro-hardness value in PMZ has the smallest value compared to the other zones.

Acknowledgements

This research is supported by the Master Program to Doctorate for Scholar Excellent (PMDSU) program of the Ministry of Research & Technology and High Education (RISTEK DIKTI) 2018 with contract number 6265/UN2.R3.1/HKP05.00/2018.

References

Aesh, M.A., 2007. Optimization of Weld Bead Dimensions in GTAW of Aluminum–Magnesium Alloy. *Materials and Manufacturing Processes,* Volume 16(5), pp. 725–736.

Alcantar-Modragón, N., Garcia, V.G., Reyes-Calderon, F., Villalobos-Brito, J.C., & Vergara-Hernández, H.J., 2021. Study of Cracking Susceptibility in Similar and Dissimilar Welds Between Carbon Steel and Austenitic Stainless Steel Through Finger Test and FE Numerical Model. *The International Journal of Advanced Manufacturing Technology,* Volume 116, pp. 2661–2686

Alcock, J., Baufeld, B., 2017. Diode Laser Welding Of Stainless Steel 304L. *Journal of Materials Processing Technology,* Volume 240, pp. 138–144

Baskoro, A.S., Masuda, R., Suga, Y., 2011. Comparison of Particle Swarm Optimization and Genetic Algorithm for Molten Pool Detection in Fixed Aluminum Pipe Welding. *International Journal of Technology,* Volume 2(1), pp. 74–83

Casalino, G., Angelastro, A., Perulli, P., Casavola, C., Moramarco, V., 2018. Study on The Fiber Laser/TIG Weldability of AISI 304 and AISI 410 Dissimilar Weld. *Journal of Manufacturing Processes,* Volume 35, pp. 216–225

Dorn, L., Devakumaran, K., Hofmann, F., 2009. Pulsed Current Gas Metal Arc Welding Under Different Shielding And Pulse Parameters; Part 1: Arc Characteristics. *ISIJ international,* Volume 49(2), pp. 251–260

Figueirôa, D.W., Pigozzo, I.O., Silva, R.H.G.E., Santos,T.F.D.A., Urtiga Filho, S.L., 2017. Influence of Welding Position and Parameters in Orbital Tig Welding Applied to Low-Carbon Steel Pipes. *Welding international,* Volume 31(8), pp. 583–590

Giridharan, P., Murugan, N., 2009. Optimization of Pulsed GTA Welding Process Parameters for The Welding of AISI 304L Stainless Steel Sheets. *The International Journal of Advanced Manufacturing Technology,* Volume 40(5-6), pp. 478–489

Gunaraj, V., Murugan, N., 2000. Prediction and Optimization of Weld Bead Volume for The Submerged Arc Process—Part 1. *Welding journal,* Volume 79(10), pp. 286s–294s

James, M.N., Matthews, L., Hattingh, D.G., 2020. Weld Solidification Cracking in A 304L Stainless Steel Water Tank. *Engineering Failure Analysis,* Volume 115, pp. 104614

Jujur, I.N., Sah, J., Bakri, A., Wargadipura, A.H.S., 2015. Analysis of Oxide Inclusions on Medical Grade 316L Stainless Steel Using Local Raw. *International Journal of Technology,* Volume 7, pp. 1184–1190

Karunakaran, N., 2012. Effect of Pulsed Current on Temperature Distribution, Weld Bead Profiles and Characteristics of GTA Welded Stainless Steel Joints. *International Journal of Engineering and Technology Science,* Volume 2 (12), pp. 1908–1916

Kou, S., 2003. Welding Metallurgy. *New Jersey, USA*, Volume 431(446), pp. 223–225

Kulkarni, S., Ghosh, P.K., Ray, S., 2008. Improvement of Weld Characteristics by Variation in Welding Processes And Parameters in Joining of Thick Wall 304LN Stainless Steel Pipe. *ISIJ international,* Volume 48(11), pp. 1560–1569

Kumar, R., Anant, R., Ghosh, P., Kumar, A., Agrawal, B., 2016. Influence of PC-GTAW Parameters on The Microstructural and Mechanical Properties of Thin AISI 1008 Steel Joints. *Journal of Materials Engineering and Performance,* Volume 25(9), pp. 3756–3765

Kumar, T.S., Balasubramanian, V., Sanavullah, M., 2007. Influences of Pulsed Current Tungsten Inert Gas Welding Parameters on The Tensile Properties of AA 6061 Aluminium Alloy. *Materials & Design,* Volume 28(7), pp. 2080–2092

Kusuma, A.P., Suhadi, A., Priadi, D., Siradj, E.S., 2017. Effect of annealing temperature on microstructure and mechanical properties of ultrafine grained brass produced by equal channel angular pressing. *International Journal of Technology,* Volume 8(1), pp. 58–65

Lothongkum, G., Viyanit, E., Bhandhubanyong, P., 2001. Study on The Effects Of Pulsed TIG Welding Parameters on Delta-Ferrite Content, Shape Factor and Bead Quality in Orbital Welding of AISI 316L Stainless Steel Plate. *Journal of Materials Processing Technology,* Volume 110(2), pp. 233–238

Manikandan, M., Arivazhagan, N., Rao, M.N., Reddy, G.M., 2014. Microstructure and Mechanical Properties of Alloy C-276 Weldments Fabricated by Continuous and Pulsed Current Gas Tungsten Arc Welding Techniques. *Journal of Manufacturing Processes,* Volume 16(4), pp. 563–572

Mirshekari, G.R., Tavakoli, E., Atapour, M., Sadeghian, B., 2014. Microstructure and Corrosion Behavior of Multipass Gas Tungsten Arc Welded 304L Stainless Steel. *Materials & Design,* Volume 55, pp. 905–911

Okano, S., Mochizuki, M., 2017. Transient Distortion Behavior During TIG Welding of Thin Steel Plate. *Journal of Materials Processing Technology,* Volume 241, pp. 103–111

Pal, K., Pal, S. K., 2011. Effect of Pulse Parameters on Weld Quality in Pulsed Gas Metal Arc Welding: A Review. *Journal of Materials Engineering and Performance,* Volume 20(6), pp. 918–931

Palani, P., Murugan, N., 2006. Selection of Parameters of Pulsed Current Gas Metal Arc Welding. *Journal of Materials Processing Technology,* Volume 172(1), pp. 1–10

Purnama, D., Winarto, W., Sofyan, N., Prihastomo, A., Ito, K., 2020. Microstructure and Mechanical Properties of Ah-36 Steel Weldment Welded Using Magnesium Modified E6013 Electrode. *International Journal of Technology,* Volume 11(1), pp. 48–59

Tseng, K.H., Hsu, C.Y., 2011. Performance of Activated TIG Process in Austenitic Stainless Steel Welds. *Journal of Materials Processing Technology,* Volume 211(3), pp. 503–512

Widyianto, A., Baskoro, A.S., Kiswanto, G., 2020. Effect of Pulse Currents on Weld Geometry and Angular Distortion in Pulsed GTAW of 304 Stainless Steel Butt Joint. *International Journal of Automotive and Mechanical Engineering,* Volume 17(1), pp. 7687–7694

Xu, J., Chen, J., Duan, Y., Yu, C., Chen, J., Lu, H., 2017. Comparison of Residual Stress Induced by TIG and LBW in Girth Weld of AISI 304 Stainless Steel Pipes. *Journal of Materials Processing Technology,* Volume 248, pp. 178–184